

Efficient single-photon frequency conversion via a giant three-level atom

Jin-Song Huang(黄劲松) and Xiang-Lin Hu(胡翔淋)

Citation: Chin. Phys. B, 2026, 35 (**6**): 060306. DOI: 10.1088/1674-1056/ae32fb
http://cpb.iphy.ac.cn; http://iopscience.iop.org/cpb

What follows is a list of articles you may be interested in

Analytical solution to incident angle quasi-phase-matching engineering for second harmonic generation in a periodic-poled lithium niobate crystal

Li-Hong Hong(洪丽红), Ya-Ting Qiu(邱雅婷), Xiao-Ni Li(李晓霓), Bao-Qin Chen(陈宝琴), and Zhi-Yuan Li(李志远)
Chin. Phys. B, 2024, 33 (**2**): 020301. DOI: 10.1088/1674-1056/ad0628

Progress and realization platforms of dynamic topological photonics

Qiu-Chen Yan(闫秋辰), Rui Ma(马睿), Xiao-Yong Hu(胡小永), and Qi-Huang Gong(龚旗煌)
Chin. Phys. B, 2024, 33 (**1**): 010301. DOI: 10.1088/1674-1056/acf284

Interaction induced non-reciprocal three-level quantum transport

Sai Li(李赛), Tao Chen(陈涛), Jia Liu(刘佳), and Zheng-Yuan Xue(薛正远)
Chin. Phys. B, 2021, 30 (**6**): 060314. DOI: 10.1088/1674-1056/abee0c

Geometric phase of an open double-quantum-dot system detected by a quantum point contact

Qian Du(杜倩), Kang Lan(蓝康), Yan-Hui Zhang(张延惠), Lu-Jing Jiang(姜露静)
Chin. Phys. B, 2020, 29 (**3**): 030302. DOI: 10.1088/1674-1056/ab6963

Performance analysis of continuous-variable measurement-device-independent quantum key distribution under diverse weather conditions

Shu-Jing Zhang(张淑静), Chen Xiao(肖晨), Chun Zhou(周淳), Xiang Wang(汪翔), Jian-Shu Yao(要建姝), Hai-Long Zhang(张海龙), Wan-Su Bao(鲍皖苏)
Chin. Phys. B, 2020, 29 (**2**): 020301. DOI: 10.1088/1674-1056/ab5efd

---

Efficient single-photon frequency conversion via a giant three-level atom

Jin-Song Huang(黄劲松)[1,2,†] and Xiang-Lin Hu(胡翔淋)[1]

[1] *School of Information Engineering, Jiangxi University of Science and Technology, Ganzhou* 341000, *China*
[2] *Key Laboratory of Low Dimensional Quantum Materials and Sensor Devices of Jiangxi Education Institutes, Ganzhou* 341000, *China*

(Received 18 August 2025; revised manuscript received 3 December 2025; accepted manuscript online 4 January 2026)

The single-photon frequency conversion in a one-dimensional waveguide coupled to a giant three-level atom is investigated. The analytical expressions of the single-photon scattering spectra are derived via the real-space Hamiltonian. Numerical results show that high-efficiency frequency conversion of single photons can be achieved by controlling the atom-waveguide coupling due to the phase-dependent interference effect of the multiple point couplings of the giant atom, and the conversion efficiency can ideally reach unity. The conversion spectra in both the Markovian and non-Markovian regimes show that multiple staggered peaks and dips emerge due to the non-Markovian retardation effect, in contrast to a single peak and dip in the Markovian regime. The influence of dissipation on the fidelity of frequency conversion is also displayed, and it shows that the fidelity is not sensitive to dissipation.

Keywords: quantum transport, scattering theory, optical waveguide, frequency conversion

PACS: 03.65.Nk, 05.60.Gg, 42.79.Gn, 42.65.Ky

DOI: 10.1088/1674-1056/ae32fb **CSTR:** 32038.14.CPB.ae32fb

1. Introduction

Photon frequency conversion refers to translating incident photons of a specified frequency into output photons of another frequency through specific physical processes,[1] which is an enabling technology applied in quantum computation[2] and quantum communication.[3] Experimentally, frequency conversion with small wavelength intervals has been implemented in many second-order and third-order nonlinear materials,[4–8] but the frequency conversion efficiencies are limited to no more than 0.5 in some of these schemes, which may restrict further potential applications.

With the development of state-of-the-art technologies, waveguide quantum electrodynamics (WQED) systems[9] have provided powerful platforms to control photon transport,[10–12] by tailoring the coupling of waveguide modes and quantum emitters effectively. In such systems, photonic waveguides are used as photon lines to connect quantum emitters, and photons are utilized as carriers to transfer quantum information between different nodes. Based on the Sagnac waveguide loop, single-photon frequency conversion approaching unity has been performed, and multi-mode quantum entanglement has also been generated via constructive interference.[13–18] Moreover, numerous investigations on high-efficiency frequency conversion of single photons have been carried out in many other physical structures, including lithium niobate materials,[19,20] chiral waveguides,[21] coupled resonator waveguides,[22,23] superconducting quantum circuits,[24] and even conversion between microwave and optical photons through atom-phonon hybrid modes in a waveguide-QED structure has also been proposed.[25]

Recently, experimental research on a giant atom in a WQED system has attracted extensive attention.[26] This kind of emitter can interact many times with the waveguide mode at multiple coupling points separated by large distances, because its size is not negligible compared to the wavelength of the propagating guided wave. Compared with the common single-point coupling of a small atom as a point mass, the multiple-point coupling of a giant atom will produce an additional phase-dependent interference effect, and thus leads to a variety of exotic quantum phenomena, including multi-frequency Fano resonance,[27–29] tunable nonreciprocal scattering,[30–32] unconditional bound states,[33–36] entanglement generation,[37,38] disentanglement dynamics,[39] directional routing[40,41] and frequency conversion.[42] Moreover, efficient nonreciprocal frequency conversion and reflectionless transport have also been demonstrated in both Markovian and non-Markovian regimes in a waveguide system coupled to a giant Λ-type atom, by varying the chiral atom-waveguide couplings.[42]

Motivated by these considerations, we study single-photon frequency conversion in a waveguide system coupled with a giant Λ-type three-level atom. In the above scheme with tunable chiral atom-waveguide couplings,[42] perfect frequency conversion is achieved by the ideal chiral case of zero couplings between the left-moving guided-wave modes and the atom, which requires the atom to be coupled only to

†Corresponding author. E-mail: jshuangjs@126.com

© 2026 Chinese Physical Society and IOP Publishing Ltd. All rights, including for text and data mining, AI training, and similar technologies, are reserved.

photons transported in a single right direction in the waveguide channel. Unlike that scheme, our proposed model focuses on high-efficiency frequency conversion by adjusting the asymmetric atom-waveguide couplings at the two coupling points of the giant atom, which is a different regulatory path with flexible coupling-direction transmission. The unequal couplings are represented by local-coupling phase parameters, which have been applied in perfectly nonreciprocal transmission and high-efficiency routing of single photons via phase-dependent interference effects.[31,32] By using a real-space approach, the scattering amplitudes of single photons are obtained analytically. Numerical results show that high-efficiency frequency conversion of a single photon can be implemented under the joint effect of the local coupling phase and the accumulated phase of the photon propagating between the two coupling points of the giant atom, and the conversion efficiency can approach unity due to the interference effect. We further analyze the single-photon frequency conversion characteristics in the Markovian regime and non-Markovian regime. It is found that multiple staggered peaks and dips emerge owing to the non-Markovian retarded effect, and the peak and dip positions dynamically shift with phase parameters, while a single peak and dip are exhibited in the conversion spectra in the Markovian regime. The fidelity of frequency conversion is also examined and can reach unity in the ideal case of no dissipation. When considering the dissipation of the atomic excited state, the fidelity decreases with the increase of dissipation. However, the fidelity is not sensitive to the dissipation, and high fidelity can still be maintained under moderate dissipation for the frequency conversion between two transition states.

2. Theoretical model

The schematic diagram of a photon converter is shown in Fig. 1. A one-dimensional waveguide is coupled to a giant Λ-type three-level atom, with two coupling points located at $x=0$ and $x=d$. The three-level atom is characterized by the excited state $|e\rangle$, metastable state $|f\rangle$, and ground state $|g\rangle$. These two atomic transitions, $|e\rangle \leftrightarrow |g\rangle$ and $|e\rangle \leftrightarrow |f\rangle$, are coupled to the waveguide modes through two coupling points located at $x=0$ and $x=d$. The corresponding coupling strengths at the two coupling points are denoted by V_{gj} and V_{fj} $(j=1,2)$, respectively. When a photon is injected into the waveguide, it will be converted between the two low-energy states by atomic scattering.

Under the rotating wave approximation, the real-space Hamiltonian[11] describing the frequency converter can be expressed as ($\hbar=1$ hereafter)

$$\begin{aligned} H \;=\; & \int \mathrm{d}x\Big[-\mathrm{i}\upsilon_g C_{\mathrm{R}}^{\dagger}(x)\frac{\partial}{\partial x}C_{\mathrm{R}}(x)+\mathrm{i}\upsilon_g C_{\mathrm{L}}^{\dagger}(x)\frac{\partial}{\partial x}C_{\mathrm{L}}(x)\Big] \\ & +(\omega_e-\mathrm{i}\gamma/2)|e\rangle\langle e|+\omega_f|f\rangle\langle f| \\ & +\sum_{j=1,2}\int \mathrm{d}x\delta[x-(j-1)d] \\ & \times\big\{[C_{\mathrm{R}}^{\dagger}(x)+C_{\mathrm{L}}^{\dagger}(x)](V_{gj}|g\rangle\langle e|+V_{fj}|f\rangle\langle e|)+\mathrm{H.c.}\big\}. \end{aligned} \tag{1}$$

Here, the ground state level has been set as the energy reference. $C_{\mathrm{L}}^{\dagger}(x)$ and $C_{\mathrm{R}}^{\dagger}(x)$ represent the creation operators for left-moving and right-moving photons in the waveguide, respectively. υ_g denotes the group velocity of the propagating photon. $\omega_{e,f}$ and γ are the transition frequency of the atomic state $|e\rangle$ ($|f\rangle$) and the intrinsic loss rate, respectively.

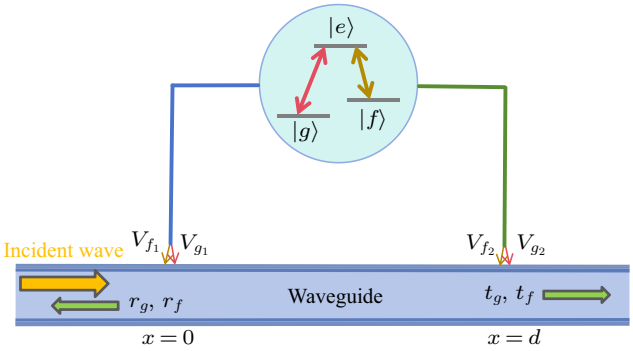


Fig. 1. Schematic view of a single-photon frequency converter consisting of a one-dimensional waveguide with a giant Λ-type atom. The giant three-level atom is coupled to the waveguide at $x=0$ and $x=d$.

Supposing that a single photon with the energy $E=\omega=\upsilon_g k$ (k being the wave number) is incident from the left port of the waveguide, and the initial state of the atom is assumed to be in the ground state $|g\rangle$, when the atom is excited by the input photon, then the atom can spontaneously decay back to $|g\rangle$ and emit a photon with the same wave vector k, or it can decay to another state $|f\rangle$ and re-emit a photon with the wave vector $q=k-\omega_f/\upsilon_g$.[42] The scattering eigenstate of the system in the single-excitation subspace can be written as

$$\begin{aligned} |\psi\rangle \;=\; & \int \mathrm{d}x[\varphi_{g\mathrm{R}}(x)C_{\mathrm{R}}^{\dagger}(x)+\varphi_{g\mathrm{L}}(x)C_{\mathrm{L}}^{\dagger}(x)]|0,g\rangle \\ & +\int \mathrm{d}x[\varphi_{f\mathrm{R}}(x)C_{\mathrm{R}}^{\dagger}(x) \\ & +\varphi_{f\mathrm{L}}(x)C_{\mathrm{L}}^{\dagger}(x)]|0,f\rangle]+\xi|0,e\rangle. \end{aligned} \tag{2}$$

Here, ξ denotes the probability amplitude of the atomic excited state. $\varphi_{g\mathrm{R},f\mathrm{R}}(x)$ and $\varphi_{g\mathrm{L},f\mathrm{L}}(x)$ are the wave functions for the right and left modes of the photon. $|0,g\rangle$ and $|0,f\rangle$ stand for the photon vacuum states with the atom in two transition states. The corresponding expressions of these wavefunctions are given by

$$\begin{aligned} \varphi_{g\mathrm{R}}(x) &= \mathrm{e}^{\mathrm{i}kx}[\theta(-x)+t_1\theta(x)\theta(d-x)+t_g\theta(x-d)], \\ \varphi_{g\mathrm{L}}(x) &= \mathrm{e}^{-\mathrm{i}kx}[r_g\theta(-x)+r_1\theta(x)\theta(d-x)], \\ \varphi_{f\mathrm{R}}(x) &= \mathrm{e}^{\mathrm{i}qx}\left[t_2\theta(x)\theta(d-x)+t_f\theta(x-d)\right], \\ \varphi_{f\mathrm{L}}(x) &= \mathrm{e}^{-\mathrm{i}qx}\left[r_f\theta(-x)+r_2\theta(x)\theta(d-x)\right]. \end{aligned} \tag{3}$$

Here, $\theta(x)$ is the step function. $t_{g,f}$ and $r_{g,f}$ represent separately the transmission and reflection amplitudes of the photon, while $t_{1,2}$ and $r_{1,2}$ describe the photon transmission and reflection amplitudes between two coupling points.

By solving the eigenvalue equation $H|\psi\rangle = E|\psi\rangle$, one can obtain the equations of motion for the probability amplitudes

$$\begin{aligned}
E\varphi_{g\mathrm{R}}(x) &= -\mathrm{i}v_g\frac{\partial}{\partial x}\varphi_{g\mathrm{R}}(x)+V_{g1}\delta(x)\xi+V_{g2}\delta(x-d)\xi,\\
E\varphi_{g\mathrm{L}}(x) &= \mathrm{i}v_g\frac{\partial}{\partial x}\varphi_{g\mathrm{L}}(x)+V_{g1}\delta(x)\xi+V_{g2}\delta(x-d)\xi,\\
E\varphi_{f\mathrm{R}}(x) &= \left(\omega_f-\mathrm{i}v_g\frac{\partial}{\partial x}\right)\varphi_{f\mathrm{R}}(x)\\
&\quad +V_{f1}\delta(x)\xi+V_{f2}\delta(x-d)\xi,\\
E\varphi_{f\mathrm{L}}(x) &= \left(\omega_f+\mathrm{i}v_g\frac{\partial}{\partial x}\right)\varphi_{f\mathrm{L}}(x)\\
&\quad +V_{f1}\delta(x)\xi+V_{f2}\delta(x-d)\xi,\\
(\omega-\omega_e+\mathrm{i}\gamma/2)\xi &= V_{g1}^*\left[\varphi_{g\mathrm{R}}(0)+\varphi_{g\mathrm{L}}(0)\right]+V_{f1}^*\left[\varphi_{f\mathrm{R}}(0)+\varphi_{f\mathrm{L}}(0)\right]\\
&\quad +V_{g2}^*\left[\varphi_{g\mathrm{R}}(d)+\varphi_{g\mathrm{L}}(d)\right]\\
&\quad +V_{f2}^*\left[\varphi_{f\mathrm{R}}(d)+\varphi_{f\mathrm{L}}(d)\right].
\end{aligned}\tag{4}$$

Substituting Eq. (3) into Eq. (4), these scattering amplitudes can be obtained as

$$\begin{aligned}
t_g &= 1-\frac{\mathrm{i}\Gamma_g[1+\mathrm{e}^{\mathrm{i}(\Delta\phi_1-\alpha_g)}][1+\mathrm{e}^{\mathrm{i}(\alpha_g-\Delta\phi_1)}]}{S(\omega)},\\
r_g &= \frac{-\mathrm{i}\Gamma_g[1+\mathrm{e}^{\mathrm{i}(\Delta\phi_1+\alpha_g)}][1+\mathrm{e}^{\mathrm{i}(\alpha_g-\Delta\phi_1)}]}{S(\omega)},\\
t_f &= \frac{-\mathrm{i}\sqrt{\Gamma_f\Gamma_g}[1+\mathrm{e}^{\mathrm{i}(\Delta\phi_2-\alpha_f)}][1+\mathrm{e}^{\mathrm{i}(\alpha_f-\Delta\phi_1)}]}{S(\omega)},\\
r_f &= \frac{-\mathrm{i}\sqrt{\Gamma_f\Gamma_g}[1+\mathrm{e}^{\mathrm{i}(\Delta\phi_2+\alpha_f)}][1+\mathrm{e}^{\mathrm{i}(\alpha_f-\Delta\phi_1)}]}{S(\omega)}.
\end{aligned}\tag{5}$$

The atom-waveguide coupling coefficients, which depend on the transition dipoles,[31] are generally complex numbers. They can be taken as $V_{g1}=V_g\mathrm{e}^{\mathrm{i}\phi_1}$, $V_{g2}=V_g\mathrm{e}^{\mathrm{i}\phi_2}$, $V_{f1}=V_f\mathrm{e}^{\mathrm{i}\phi_3}$, and $V_{f2}=V_f\mathrm{e}^{\mathrm{i}\phi_4}$, with local coupling phases $\phi_{1,2,3,4}$. Thus, the phase differences are $\Delta\phi_1=\phi_2-\phi_1$ and $\Delta\phi_2=\phi_4-\phi_3$. $\Gamma_g=V_g^2/v_g$ and $\Gamma_f=V_f^2/v_g$ are the atomic emission rates into the waveguide. $\alpha_g=kd$ and $\alpha_f=qd$ are the accumulated phases of the photons propagating between two coupling points. $\Delta\omega=\omega-\omega_e$ is the frequency detuning, and $S(\omega)=\Delta\omega+\mathrm{i}\gamma/2+2\mathrm{i}\Gamma_g(1+\mathrm{e}^{\mathrm{i}\alpha_g}\cos\Delta\phi_1)+2\mathrm{i}\Gamma_f(1+\mathrm{e}^{\mathrm{i}\alpha_f}\cos\Delta\phi_2)$.

3. Single-photon frequency conversion via a giant atom

In the coupled giant atom-waveguide system, $\alpha_g=kd=\omega_e\tau+\Delta\omega\tau$ and $\alpha_f=qd=(\omega_e-\omega_f)\tau+\Delta\omega\tau$ are the accumulated phases of photons between two coupling points, with $\tau=d/v_g$ the corresponding propagation time. For a fixed separation between two coupling points, the accumulated phase can be regarded as a constant part $\alpha_{g0}=\omega_e\tau$ [$\alpha_{f0}=(\omega_e-\omega_f)\tau$] and a detuning-dependent part.[32,42–45] Consequently, we will study the single-photon scattering in both the Markovian and the non-Markovian regimes, depending on whether the propagation time τ can be neglected or not.

We first consider the Markovian regime where the propagation time τ is sufficiently small such that $\alpha_{g,f}\approx\alpha_{g0,f0}$ is approximately constant. In the coupled waveguide system, the transport characteristics of a single photon are governed by the scattering probabilities $T_{g(f)}=|t_{g(f)}|^2$ and $R_{g(f)}=|r_{g(f)}|^2$. Figure 2(a) shows the photon transmission at two ports with no dissipation. It is obvious that the photon flow satisfies the conservation relation of $T_g+T_f+R_g+R_f=1$ (see the yellow straight line). Here, all parameters are normalized by Γ_g except the phases. $\Gamma_g=\Gamma_f$, $\alpha_g=\alpha_f+2n\pi=\alpha$, and $\Delta\phi_1=\Delta\phi_2=\Delta\phi$ are assumed for simplification, with n an integer. As seen, the transmission on the left port is completely blocked over the entire frequency domain under the condition of $\Delta\phi=\alpha=(2m+1)\pi/2$ with m an integer, as shown by the red dashed line and green dotted line. $R_g=R_f=0$ results from the asymmetric coupling by controlling the unequal local coupling phases, which closes the left coupling channel. Consequently, a complete conversion is achieved at the resonance point.

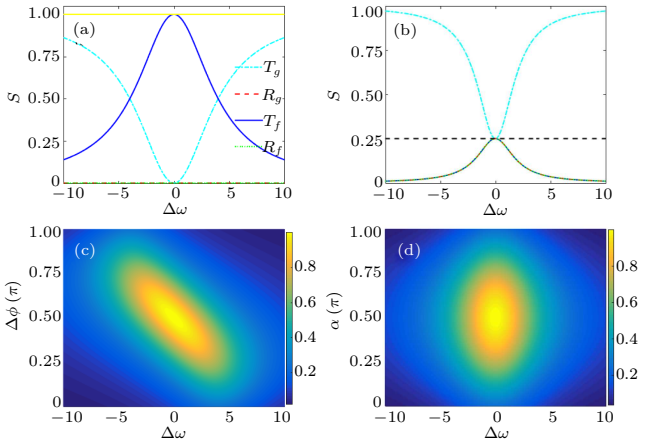


Fig. 2. In the Markovian regime, the scattering probabilities S, including T_g (dash dotted cyan curves), T_f (solid blue curves), R_g (dashed red curves), and R_f (dash dotted green curves), for a giant atom in (a) and for a small atom in (b). Here, the curves of R_g and R_f overlap each other in (a) due to $R_g=R_f=0$, while the curves of T_f, R_g and R_f overlap each other in (b) due to $R_g=R_f=T_f$. T_f as a function of the detuning $\Delta\omega$, and the phase $\Delta\phi$ in (c) and the phase α in (d). The yellow straight line in (a) denotes the total photon transmission probability with the conservation relation. For convenience, all parameters are in units of Γ_g except the phases. These parameters are $\Gamma_f=\Gamma_g=1$, $\gamma=0$. $\Delta\phi=\alpha=\pi/2$ in (a), $\alpha=\pi/2$ in (c), and $\Delta\phi=\pi/2$ in (d).

For comparison, we also study the small-atom model in Fig. 2(b), which has only one coupling point at $x=0$, and the coupling at $x=d$ is zero. The incident photon flows to two ports, and the photon probability is equal at $T_f=R_f=T_g=R_g=0.25$ at the resonance point, where T_f reaches the maximum value of 0.25. Note that the single small-atom case has

been investigated by Obi and Shen,[46] where the sum conversion probability of the input photon is $T_f + R_f = 0.5$. Of course, when more emitters are considered, high-efficiency conversion can be achieved by scattering from multiple emitters due to the interference effect caused by the spatial multi-point coupling, which has been demonstrated for similar polarization conversion in coupled waveguide systems with two emitters[47] and an array of three-level emitters.[48] Thus, efficient frequency conversion can be achieved by a giant atom with two coupling points, with a simple structure in contrast to the multiple-emitter cases. Furthermore, we investigated the influence of the phases on T_f in Figs. 2(c) and 2(d). It can be seen that two wide elliptical regions of high conversion efficiency $T_f > 0.9$ appear near $\Delta\phi = \alpha = \pi/2$ and the resonance point, and conversion peaks for T_f approaching 1 are displayed at the two center points, respectively. Therefore, effective frequency conversion can be achieved by varying the phases to generate asymmetric coupling.

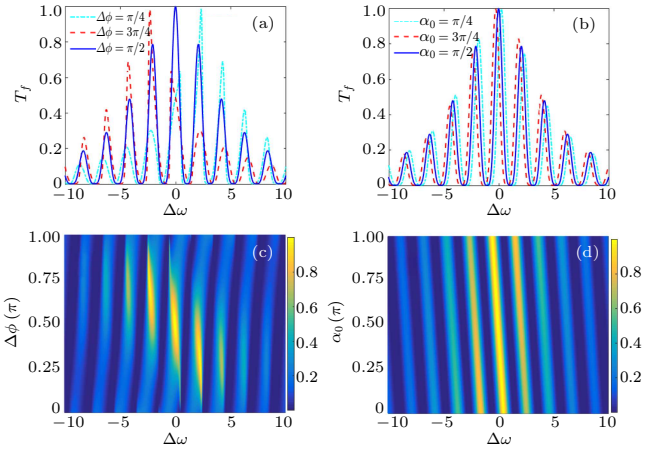


Fig. 3. The T_f versus the detuning $\Delta\omega$ for different phases in the non-Markovian regime. (a) $\alpha_0 = \pi/2$, $\Delta\phi = \pi/4$ (dash-dotted cyan curve), $\Delta\phi = 3\pi/4$ (dashed red curve), and $\Delta\phi = \pi/2$ (solid blue curve). (b) $\Delta\phi = \pi/2$, $\alpha_0 = \pi/4$ (dash-dotted cyan curves), $\alpha_0 = 3\pi/4$ (dashed red curves), $\alpha_0 = \pi/2$ (solid blue curves). T_f as a function of the detuning $\Delta\omega$, and the phase $\Delta\phi$ in (c) and the phase α_0 in (d), where $\alpha_0 = \pi/2$ and $\Delta\phi = \pi/2$ are separately set in (c) and (d). The other parameters are $\tau = 3\Gamma_g$, $\Gamma_g = \Gamma_f$, and $\gamma = 0$.

Then we consider the non-Markovian regime, where the propagation time τ of the photon in the waveguide cannot be neglected and α has a strong dependence on the detuning $\Delta\omega$. Figures 3(a) and 3(b) display T_f as a function of the detuning $\Delta\omega$ when one of the two phases $(\alpha_0, \Delta\phi)$ is fixed at $\pi/2$, and the other is taken as $\pi/4$, $3\pi/4$, and $\pi/2$. Due to the time delay effect, more complicated oscillating transmission spectra appear, showing multiple staggered peaks and dips. It can be observed that the positions of these dips are located at $\Delta\omega = [(2m+1)\pi - \alpha_0 - \Delta\phi]/\tau$, while the peak positions are located at $\Delta\omega = [(2m+1)\pi - \alpha_0 + \Delta\phi]/\tau$. Here, $\alpha_0 = \alpha_{g0} = \alpha_{f0} + 2n\pi$ has been assumed above for simplification. Thus, the frequency positions corresponding to these transmission peaks and dips will move with the change in the two phases. To observe more notable features, T_f as a function of the frequency detuning $\Delta\omega$ and the two phases is plotted in Figs. 3(c) and 3(d), respectively. As can be seen, three bright oblique strip-shaped regions presenting high T_f values appear asymmetrically on both sides of the resonance point. In the middle region, the center frequency of the maximum peak shifts linearly with the variation. The other two asymmetric regions arise due to the combined effect of the phases and the detuning.

For the ideal condition, there is no dissipation during propagation. However, in a practical system, atomic decay is unavoidable, and thus the influence of dissipation on the frequency conversion should be studied. Figure 4 describes the photon frequency conversion in the presence of dissipation for three different dissipation values $\gamma = 0, 1, 6$. In the ideal lossless case, the total photon flow is conserved and exchanges occur between T_f and T_g. With increasing dissipation strength, the loss of the photon flow also occurs, and T_f and T_g gradually decrease, as shown in Fig. 4(a). Note that near the resonance point, there exists a probability of T_g for large dissipation. This is because for strong dissipation, the resonance excitation of the $|e\rangle \leftrightarrow |g\rangle$ transition weakens. Compared with the complete conversion with $T_g = 0$ when there is no dissipation, only a small part of the excited photons is transformed, and thus a part is retained.

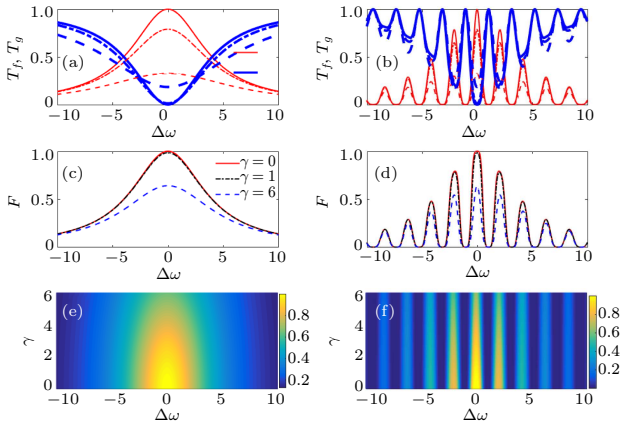


Fig. 4. The T_g (thick blue curves) and T_f (fine red curves) versus the detuing $\Delta\omega$ for different dissipations: $\gamma = 0$ for solid lines, $\gamma = 1$ for dash-dotted line, and $\gamma = 6$ for dashed lines in (a) and (b). F versus the detuning $\Delta\omega$ for different dissipations in (c) and (d). F as a function of the detuning $\Delta\omega$ and the dissipation γ in (e) and (f). Left panels (a), (c) and (e) display the transmission features in the Markovian regime, right panels (b), (d) and (f) correspond to the non-Markovian regime. $\alpha_0 = \Delta\phi = \pi/2$. The other parameters are the same as those in Fig. 2.

To compare the conversion of the two frequencies at the single right port, we define a fidelity $F = T_f/(T_f + T_g)$, which represents the ratio of the converted photon transmission to the total right transmission.[49] For $F = 0$, the transmitted photon is the original transition one, while $F = 1$ implies that the two frequencies are completely converted. Figure 4(c) displays that a general dissipation $\gamma = 1$, which is comparable with the atomic emission rate, gives rise to a high fidelity of

$F = 0.98$ near the resonance point. Thus, the fidelity is robust and undergoes only a minor change compared to the ideal case. This indicates that dissipation does not have a strong impact on the frequency switch. A significant effect occurs only for very strong dissipation, such as $F = 0.64$ for $\gamma = 6$ near the resonance point. F as a function of γ and $\Delta\omega$ is also plotted in Fig. 4(e). It is shown that there exists a bright elliptical region with high fidelity at the resonance point in the dissipation-value range from 0 to about 3, which further shows that in the presence of larger dissipation, high fidelity continues to be maintained. Correspondingly, the right panels of Figs. 4(b), 4(d), and 4(f) present a comparison with the left panels in the non-Markovian case. They have similar features to the left panels, except that multiple staggered peaks and dips emerge in comparison to the single peak and dip.

Similarly, Fig. 5 displays the influence of different phases and the dissipation on T_f, T_g, and the fidelity at the resonance point. When $\Delta\omega = 0$, there is no difference for these two cases in both Markovian and non-Markovian regimes. It can be found that there are conclusions similar to those in Fig. 4: high-fidelity regions appear in the vicinity of both phases being $\pi/2$, and the fidelity is not sensitive to the atomic decay, as seen in the $(\Delta\phi, \gamma)$ and (α, γ) panels.

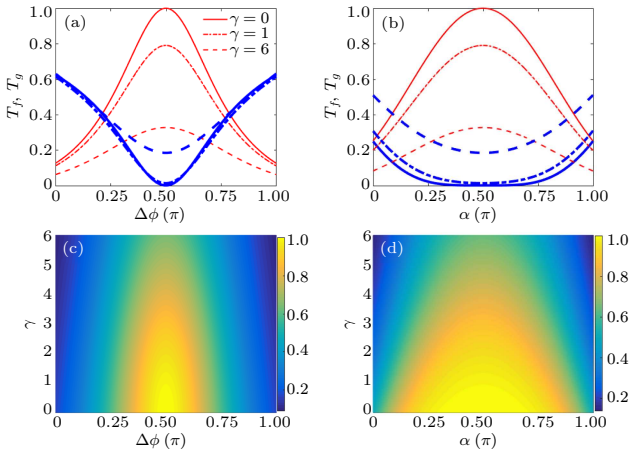


Fig. 5. The T_g (thick blue curves) and T_f (fine red curves) versus the phase $\Delta\phi$ in (a) and α in (b) for different dissipations: $\gamma = 0$ for solid lines, $\gamma = 1$ for dash-dotted line, and $\gamma = 6$ for dashed lines. F as a function of the dissipation γ, and the phase $\Delta\phi$ in (c) and α in (d). $\alpha = \pi/2$ in (a) and (c). $\Delta\phi = \pi/2$ in (b) and (d). Other parameters are the same as those in Fig. 2.

The physical implementation of our scheme should be remarked. The proposal can be realized experimentally in a current circuit QED system,[31] where the giant atom can be a superconducting qubit and a superconducting transmission line is used as the waveguide.[50] The two-point atom–waveguide coupling can be performed by coupling an Xmon qubit to the transmission line waveguide at two different locations.[51,52] The accumulated phase can be implemented by tuning the qubit frequency, and the local coupling phases between the giant atom and the waveguide can be controlled by using Josephson-junction loops threaded by external fluxes.[53] For instance, the experimental parameters can be selected as $(\Gamma_g, \gamma) = 2\pi \times (7.38, 0.02)$ MHz.[50,54] It is found that the decay of the qubit is significantly less than the coupling, and thus efficient frequency conversion can be achieved.

4. Conclusion

In summary, we have investigated single-photon frequency conversion via a giant Λ-type three-level atom scattering in a one-dimensional waveguide. High conversion efficiency at two transition frequencies can be effectively achieved by varying the phase parameters. The frequency conversion spectra in both the Markovian and non-Markovian regimes show that multiple staggered peaks and dips emerge due to the non-Markovian retarded effect, while a single peak and dip occur in the Markovian regime. High fidelities of these conversions are also examined when dissipation is considered, which shows that the fidelity is robust against atomic decay. Therefore, the proposed converters may have wide potential in quantum computation and quantum information processing.

Acknowledgements

Project supported by the National Natural Science Foundation of China (Grant No. 12365003), Key Laboratory of Low Dimensional Quantum Materials and Sensor Devices of Jiangxi Education Institutes (Grant No. GanJiaoKeZi-20241301), and Jiangxi Provincial Natural Science Foundation (Grant No. 20212BAB201014).

References

[1] Huang J M and Kumar P 1992 *Phys. Rev. Lett.* **68** 2153
[2] Langford N K, Ramelow S, Prevedel R, Munro W J, Milburn G J and Zeilinger A 2011 *Nature* **478** 360
[3] Gisin N and Thew R 2007 *Nat. Photonics* **1** 165
[4] Ramelow S, Fedrizzi A, Poppe A, Langford N K and Zeilinger A 2012 *Phys. Rev. A* **85** 013845
[5] Ma B, Wei S H, Chen Z S, Shang X J, Ni H Q and Niu Z C 2018 *Chin. Phys. B* **27** 097802
[6] Zhang X T 2021 *Chin. Phys. B* **30** 014205
[7] Qi X Z and Ren X F 2022 *Chin. Phys. B* **31** 104203
[8] Zhao C, Wu C, Zhu P Y, Du Y X, Wang Y, Yu M M, Zhang K K and Xu P 2025 *Chin. Phys. B* **34** 014206
[9] Goban A, Hung C L, Yu S P, Hood J D, Muniz J A, Lee J H, Martin M J, McClung A C, Choi K S, Chang D E, Painter O and Kimble H J 2014 *Nat. Commun.* **5** 3808
[10] Shen J T and Fan S 2005 *Phys. Rev. Lett.* **95** 213001
[11] Shen J T and Fan S 2009 *Phys. Rev. A* **79** 023837
[12] Zhou L, Gong Z R, Liu Y X, Sun C P and Nori F 2008 *Phys. Rev. Lett.* **101** 100501
[13] Bradford M, Obi K C and Shen J T 2012 *Phys. Rev. Lett.* **108** 103902
[14] Bradford M and Shen J T 2021 *Phys. Rev. A* **85** 043814
[15] Chen H Y and Liu J B2014 *J. Phys. B: At. Mol. Opt. Phys.* **47** 245503
[16] Zheng A S, Zhang G Y, Gui L W and Liu J B 2015 *Laser Phys.* **25** 065201
[17] Ma Y F, Li T P and Zheng A S 2018 *Phys. Rev. A* **28** 075202
[18] Du L and Li Y 2021 *Phys. Rev. A* **104** 023712
[19] Wang X, Jiao X F, Wang B, Liu Y, Xie X P, Zheng M Y, Zhang Q and Pan J W 2023 *npj Inf. Process.* **9** 38
[20] M Schäfer M, Kambs B, Herrmann D, Bauer T and Becher C 2025 *Adv. Quantum Technol.* **8** 2300228

[21] Shi C, Cheng M T, Ma X S, Wang D, Huang X S, Wang B and Zhang J Y 2018 *Chin. Phys. Lett.* **35** 054202
[22] Wang Z H, Zhou L, Li Y and Sun C P 2014 *Phys. Rev. A* **89** 053813
[23] Xu X W, Chen A X, Yong Li Y and Liu Y X 2017 *Phys. Rev. A* **96** 053853
[24] Jia W Z, Wang Y W and Liu Y X 2021 *Phys. Rev. A* **96** 053832
[25] Cao M S and Jia W Z 2021 *J. Phys. B: At. Mol. Opt. Phys.* **54** 055502
[26] Manenti R, Kockum A F, Patterson A, Behrle T, Rahamim J, Tancredi G, Nori F and Leek P J 2017 *Nat.Commun.* **8** 975
[27] Feng S L and Jia W Z 2021 *Phys. Rev. A* **104** 063712
[28] Peng Y P and Jia W Z 2023 *Phys. Rev. A* **108** 043709
[29] Liu J Y, Jin J W, Liu H Y, Ming Y and Yang R C 2023 *Quantum Inf. Process.* **22** 74
[30] Wang Z, Du L, Li Y and Liu Y 2019 *Phys. Rev. A* **100** 053809
[31] Li H Z, Zhang X P, Zeng R, Hu M, Xu M M, Zhou X F, Xia X W, Xu J P and Yang Y P 2024 *Opt. Express* **32** 38292
[32] Chen Y T, Du L, Guo L, Wang Z, Zhang Y, Li Y and Wu J H 2022 *Commun. Phys.* **5** 215
[33] Zhao W and Wang Z 2020 *Phys. Rev. A* **101** 053855
[34] Guo L, Kockum A F, Marquardt F and Johansson G 2020 *Phys. Rev. Res.* **2** 043014
[35] Xiao H, Wang L, Li Z H, Chen X and Yuan L 2022 *npj Quantum Inf.* **8** 80
[36] Sun G, Yang Y, Li J, Jing Lu J and Zhou L 2025 *Phys. Rev. A* **111** 033701
[37] Yu H, Wang Z and Wu J H 2021 *Phys. Rev. A* **104** 013720
[38] Santos A C and Bachelard R 2023 *Phys. Rev. Lett.* **130** 053601
[39] Yin X L, Luo W B and Liao J Q 2022 *Phys. Rev. A* **106** 063703
[40] Zhou J, Yin X L and Liao J Q 2023 *Phys. Rev. A* **107** 063703
[41] Wang X, Yang W X, Chen A X, Li L, Shui T, Li X and Wu Z 2022 *Quantum Sci. Technol.* **7** 015025
[42] Du L, Chen Y T and Li Y 2021 *Phys. Rev. Res.* **3** 043226
[43] Guo L, Grimsmo A, Kockum A F, Pletyukhov M and Johansson G 2017 *Phys. Rev. A* **95** 053821
[44] Andersson G, Suri B, Guo L, Aref T and Delsing P 2019 *Nat. Phys.* **15** 1123
[45] Yin X L, Liu Y H, Huang J F and Liao J Q 2022 *Phys. Rev. A* **106** 013715
[46] Obi K C and Shen J T 2015 *Opt. Commun.* **343** 135
[47] Cheng M T, Xia X W, Xu J P, Zhu C J, Wang B and Ma X S 2018 *Opt. Express* **26** 28872
[48] Zhang Z Y, Dong Y L, Zhang S L and Zhu S Q 2013 *Opt. Express* **21** 20786
[49] Bai Y F, Zhai S Q, Gao J R and Zhang J X 2011 *Chin. Phys. B* **20** 034207
[50] Blais A, Huang R S, Wallraff A, Girvin S M and Schoelkopf R J 2004 *Phys. Rev. A* **69** 062320
[51] Vadiraj A M, Ask A, McConkey T G, Nsanzineza I, Sandbo Chang C W, Kockum A F and Wilson C M 2021 *Phys. Rev. A* **103** 023710
[52] Kannan B, Ruckriegel M J, Campbell D L, Kockum A F, Braumüller J, *et al.* 2020 *Nature* **583** 775
[53] Wang X and Li H R 2022 *Quantum Sci. Technol.* **7** 035007
[54] Huang J S, Wei L F and Oh C H 2011 *Phys. Rev. A* **83** 032110